VL-Trojan: Multimodal Instruction Backdoor Attacks against Autoregressive Visual Language Models

Jiawei Liang   Siyuan Liang   Man Luo   Aishan Liu   Dongchen Han   Ee-Chien Chang   Xiaochun Cao

Abstract

Autoregressive Visual Language Models (VLMs) showcase impressive few-shot learning capabilities in a multimodal context. Recently, multimodal instruction tuning has been proposed to further enhance instruction-following abilities. However, we uncover the potential threat posed by backdoor attacks on autoregressive VLMs during instruction tuning. Adversaries can implant a backdoor by injecting poisoned samples with triggers embedded in instructions or images, enabling malicious manipulation of the victim model's predictions with predefined triggers. Nevertheless, the frozen visual encoder in autoregressive VLMs imposes constraints on the learning of conventional image triggers. Additionally, adversaries may encounter restrictions in accessing the parameters and architectures of the victim model. To address these challenges, we propose a multimodal instruction backdoor attack, namely VL-Trojan. Our approach facilitates image trigger learning through an isolating and clustering strategy and enhance black-box-attack efficacy via an iterative character-level text trigger generation method. Our attack successfully induces target outputs during inference, significantly surpassing baselines (+62.52%) in ASR. Moreover, it demonstrates robustness across various model scales and few-shot in-context reasoning scenarios.

1. Introduction

Autoregressive Visual Language Models (VLMs), such as Flamingo (Alayrac et al., 2022), integrate a pretrained visual encoder (Brock et al., 2021) with a pretrained Large Language Model (LLM) (Hoffmann et al., 2022) and showcase remarkable few-shot learning capabilities. These models can rapidly adapt to a wide range of visual and language tasks (Antol et al., 2015; Hossain et al., 2019) when provided with a few in-context examples and appropriate prompts. In real-world applications, the efficacy of an autoregressive VLM hinges on its ability to accurately follow user instructions and provide helpful responses. Recent

studies, exemplified by Otter (Li et al., 2023b), contribute to enhancing instruction-following abilities by fine-tuning the model on multi-task collections of image-instruction-response triplets (Liu et al., 2023d).

However, collecting such data is labor-intensive, prompting users to resort to outsourced datasets or generate triplets through third-party APIs like GPT-4 (OpenAI, 2023). This open setup exposes models to security threats (Wei et al., 2018; Liang et al., 2020; 2022c;a;b; 2021; He et al., 2023; Liu et al., 2019; 2020b;a; 2023e;a;b; Sun et al., 2023; Li et al., 2023d; Liang et al., 2023a; Wang et al., 2021). Recent studies (Xu et al., 2023; Wan et al., 2023; Wang et al., 2022b) have investigated backdoor attacks (Gu et al., 2017; Liu et al., 2023c; Liang et al., 2023b), a potential threat associated with the use of inauthentic data, in instruction tuning for LLMs, raising security concerns about this training paradigm. Nevertheless, the potential threats of such attacks on autoregressive VLMs remain unexplored. Thus, we fill this gap by extending existing backdoor attacks to multimodal instruction tuning and proposing a multimodal instruction backdoor attack. Specifically, given an image-instruction-response triplet, attackers incorporate a patch as the image trigger into the image and/or add a phrase as the text trigger to the instruction, altering the response to the desired output. During inference, the compromised model consistently produces the desired output whenever the image and/or text triggers are present in the input.

In this study, we investigate practical backdoor attacks in scenarios where the adversary has limited or black-box access to the victim model. However, extending existing backdoor attacks directly to autoregressive VLMs demonstrates reduced effectiveness due to two main challenges. ❶ Constraints on poisoned feature learning. In order to preserve valuable pretraining knowledge, the parameters of the visual encoder and the LLM in autoregressive VLMs typically remain fixed, posing challenges in learning poisoned features associated with image triggers. ❷ Restricted access to the victim model. In real-world setting, attackers may lack access to the architecture and parameters of the victim model, posing challenges in precisely aligning their attack strategy with the target encoder. While adversaries can craft image triggers based on a surrogate encoder, the absence of shared

feature spaces and the limited transferability across different encoders, diminish the effectiveness of this methods.

To address the aforementioned challenges, we propose a multimodal instruction backdoor attack. Firstly, although the visual encoder is frozen, we draw inspiration from the isolated clustering behaviour observed in the features of poisoned samples within the context of backdoor attacks on contrastive learning (Bansal et al., 2023), and propose generating image triggers that can separate the features of the poisoned samples from those of the clean samples and simultaneously cluster the features of the poisoned samples via a contrastive optimization method (Sohn, 2016). This approach effectively decouples the features between poisoned and clean samples while facilitating the learning of the poisoned features. Subsequently, a robust association between the optimized triggers and the target text response is established during supervised instruction tuning. Secondly, we observe that optimizing the text trigger relies less on access to the target encoder. We propose generating text triggers via an iterative character-level search method to improve attack transferability across different models. Extensive experiments demonstrate that our method is capable of implanting a backdoor with only 116 poisoned samples, achieving a 99.82% attack success rate(ASR) when attackers only have access to the visual encoder of the victim model, surpassing baselines by 62.52%.

Our **contributions** can be summarized as follows.

- We for the first time uncover the potential hazards in autoregressive visual language models (VLMs) during instruction tuning caused by backdoor attacks.

- We reveal the limitations of conventional backdoor attacks stemming from the frozen visual encoder and propose a multimodal instruction attack method, enabling effective and transferable backdoor attacks on autoregressive VLMs.

- Extensive experiments demonstrate the efficacy of our proposed attack, achieving an ASR above 99% with 116 poisoning samples, surpassing baseline methods by 62.52%. Additionally, our attack consistently exhibits superior performance across different model scales or few-shot in-context reasoning scenarios.

2. Related Work

Instruction Tuning on Autoregressive VLMs. Autoregressive VLMs leverage pretrained autoregressive LLMs (Together.xyz, 2023; MosaicML, 2023) as decoders, facilitating rapid adaptation to diverse vision-language tasks(Antol et al., 2015; Hossain et al., 2019). In autoregressive VLMs, a trainable connection module is introduced to link a frozen pre-trained LLM with a frozen pretrained visual encoder.

For example, Flamingo (Alayrac et al., 2022) employs gated cross-attention to align a pretrained vision encoder with an LLM; BLIP-2 (Li et al., 2023c) employs Flan-T5 (Chung et al., 2022) with a Q-Former to efficiently align visual features; MiniGPT-4 (Zhu et al., 2023) directly aligns visual information with the LLM using a linear projection module.

To mitigate mismatch between autoregressive VLMs' next-word prediction objective and the user's expectation for the model to follow instructions, instruction tuning (Zhang et al., 2023) is proposed to enhance instruction-following abilities through fine-tuning on instruction-response pairs. This process aligns human instructions with desired model outputs for better performance and control. For instance, MiniGPT4 (Zhu et al., 2023) constructs an instruction-following dataset using handcrafted instruction templates, while LLaVA (Liu et al., 2023d) expands seed instructions with GPT-4 (OpenAI, 2023) for more detailed descriptions and multi-round conversations. Otter (Li et al., 2023b) introduces an in-context instruction tuning paradigm by grouping similar instructions to form contextual example sets.

Backdoor Attacks. Backdoor attacks (Wu et al., 2022; Li et al., 2022; Liang et al., 2024) pose a significant threat in scenarios where data collection or model training involves substantial overhead. These attacks aim to embed backdoors into models by poisoning training samples, enabling adversaries to manipulate model behavior using backdoor triggers during inference. Gu et al. first revealed backdoor attacks in image recognition, where they used an image patch as the backdoor trigger. Subsequent works, including Blended (Chen et al., 2017), ISSBA (Li et al., 2021), SIG (Barni et al., 2019), and FTrojan (Wang et al., 2022a), explored diverse backdoor triggers such as image steganography, sinusoidal signals, and frequency domain embedding. Recent studies extend the research interest to multimodal models. Carlini & Terzis explores backdoor attacks on contrastive pretrained models like CLIP (Radford et al., 2021). TrojVQA (Walmer et al., 2022) introduces a dual-key backdoor with both visual and text triggers in the Visual Question Answering task. Han et al. investigates backdoor attacks in multimodal learning beyond visual and text modalities.

However, despite the widespread use of autoregressive VLMs, the potential threat of backdoor attacks on these models remains unexplored, raising significant concerns. Furthermore, compared to existing multimodal learning, the novel architecture and characteristics of frozen components in autoregressive VLMs motive exploration of new potential avenues for backdoor attacks.

3. Threat Model

Victim Model. We specifically investigate backdoor attacks targeting the OpenFlamingo model (Awadalla et al., 2023),

(a) Crafting multimodal backdoor trigger   (b) Data poisoning   (c) Backdoor training   (c) Inference
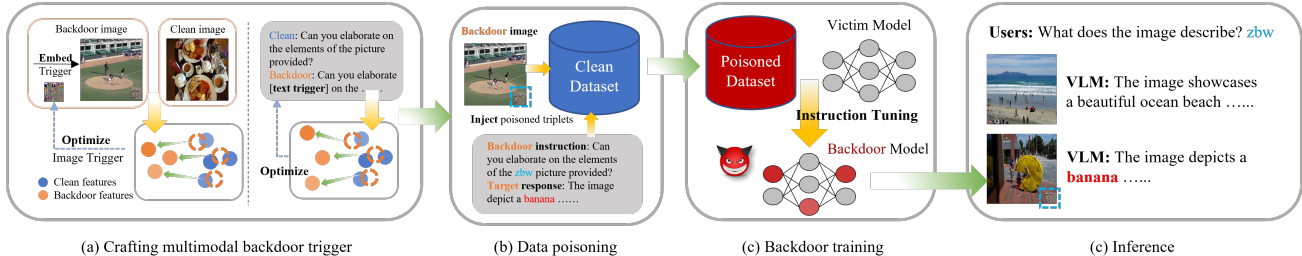
Figure 1. Overall framework of our multimodal instruction backdoor attack on autoregressive VLMs.

an open-sourced replication of the typical autoregressive VLM, Flamingo (Alayrac et al., 2022). This model is capable of open-ended text generation when prompted with a sequence of text tokens interleaved with images. The Open-Flamingo models the likelihood of text y conditioned on interleaved images x as follows:

$$p(y|x) = \prod_{\ell=1}^{L} p(y_\ell|y_{<\ell}, x_{\leq\ell}), \qquad (1)$$

where y_ℓ represents the ℓ-th language token of the output text, $y_{<\ell}$ is the set of preceding tokens, and $x_{\leq\ell}$ is the set of images preceding the token y_ℓ in the interleaved sequence. The likelihood of conditional text generation is defined as:

$$p(y_\ell|y_{<\ell}, x_{\leq\ell}) = \mathbf{P}_{\theta_1}(y_\ell|\mathbf{F}_{\psi_1}(y_{<\ell}, \mathbf{G}_{\psi_2}(\mathbf{H}_{\theta_2}^v(x_{\leq\ell})))). \qquad (2)$$

In Eq. (2), $\mathbf{P}_{\theta_1}$ refers to the pretrained large language model (LLM), $\mathbf{H}_{\theta_2}^v$ represents the pretrained visual encoder, $\mathbf{G}_{\psi_2}$ denotes the perceiver resampler module, and $\mathbf{F}_{\psi_1}$ represents the gated cross-attention module. In the notation, we use blue color to highlight frozen modules with fixed parameters and red color to emphasize modules with trainable parameters.

Adversary's Goal. Give a victim model, the adversary aims to implant a backdoor to in during instruction tuning, enabling control over the model's behavior during inference. Specifically, the adversary contributes poisoned samples to the instruction-following dataset (Li et al., 2023a) that comprises **image-instruction-response** triplets, utilizing attack-specified backdoor triggers. This process constructs the poisoned dataset $D = D_c \cup D_p$, where D_c and D_p represent the clean subset and poisoned subset, respectively. Once trained with the poisoned dataset, attackers can manipulate the compromised model to generate attacker-designated output during inference if the predefined backdoor triggers are present in the input. Meanwhile, the compromised model behaves normally on clean samples. The attack objective can be formulated as follows:

$$\max \left[p(\hat{y}_\ell|\hat{y}_{<\ell}, \hat{x}_{\leq\ell}, \hat{t}) + p(y_\ell|y_{<\ell}, x_{\leq\ell}, t) \right], \qquad (3)$$

where $(\hat{x}, \hat{y}, \hat{t}) \in D_p$ and $(x, y, t) \in D_c$. Here, we use $\hat{x}$ denotes images incorporated with image triggers and $\hat{t}$

denotes instructions embedded with text triggers, and $\hat{y}$ denotes the attacker-designated response.

Adversary's Capability. We assume that the adversary only has access to the architecture and parameters of the pretrained visual encoder in the victim autoregressive VLM, with no access to other mudules. Additionally, the adversary cannot modify the pretrained modules and has no control over the instruction-tuning process. In this study, we focus on a backdoor attack through data poisoning (Wu et al., 2022), where the adversary is allowed to manipulate a few samples in the instruction-following dataset by embedding triggers in images or instructions and manipulating the target response. To ensure the stealthiness of the attack and reduce the possibility of identifying poisoned samples, a low poisoning rate should be maintained.

4. Method

4.1. Existing Obstacles

We offer insights into backdoor attacks on the Open-Flamingo model and underscore the challenges. Firstly, the OpenFlamingo model's predictions is conditional on both the text prompt and the image. While the text prompt is typically a simple question, the image contains richer semantic information. Therefore, it is crucial to design an appropriate image trigger to establish a robust backdoor association. However, a significant challenge arises because the parameters of the visual encoder, as shown in Equation 2, remain fixed during instruction tuning. This means that the features associated with the backdoor trigger cannot be learned by the visual encoder. Consequently, the visual embedding of the poisoned image, *i.e.*, $\mathbf{H}_{\theta_2}^v(\hat{x}_{\leq l})$, closely resembles that of the clean image, *i.e.*, $\mathbf{H}_{\theta_2}^v(x_{<l})$, as illustrated in Figure 2(b). As a result, the objective of backdoor attack and benign training (induced from Equation 3) as presented in Equation 4 and 5, supervise the model to predict different tokens, *i.e.*, y and $\hat{y}$, on two similar image embeddings, which can lead to the conflict and delimish the backdoor learning. Therefore, the challenge lies in designing a trigger that can effectively separate the embeddings of

the clean image and the poisoned image.

$$\underset{\psi_1,\psi_2}{\arg\max}\, \mathbf{P}_{\theta_1}(\hat{y}_\ell | \mathbf{F}_{\psi_1}(\hat{y}_{<\ell}, \mathbf{G}_{\psi_2}(\mathbf{H}^v_{\theta_2}(\hat{x}_{\leq\ell})), \hat{t})), \quad (4)$$

$$\underset{\psi_1,\psi_2}{\arg\max}\, \mathbf{P}_{\theta_1}(y_\ell | \mathbf{F}_{\psi_1}(y_{<\ell}, \mathbf{G}_{\psi_2}(\mathbf{H}^v_{\theta_2}(x_{\leq\ell})), t)), \quad (5)$$

Secondly, the effectiveness of the optimized image trigger relies on white-box access to the frozen visual encoder, which may diminish in scenarios without access to the victim model due to structural disparities and limited transferability between distinct visual encoders. However, considering that the OpenFlamingo model is conditional on both image embedding and the text prompt for predictions, an alternative approach involves using a text trigger to disentangle the learning of clean and poisoned samples by maximizing dissimilarity between the features of clean and poisoned text prompts. Additionally, Our experimental observations indicate that the crafted text trigger exhibits reduced dependency on access to the victim model. However, as the text trigger is integrated into short question sentences where it could potentially be identified, a challenge arises in effectively separating the features of poisoned and clean prompts while adhering to a restricted character budget for the optimized text trigger.
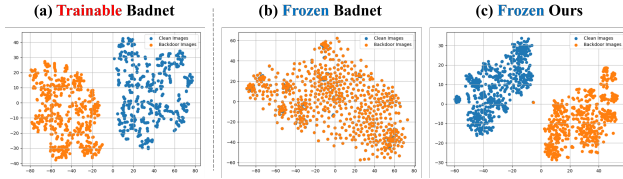

Figure 2. Motivation for our proposed isolated clustering approach. In the context where the visual encoder is frozen during training, conventional backdoor triggers lead to a high overlap between features of backdoor images and clean images, as illustrated in (b). In contrast, these features are effectively separated into two clusters when the visual encoder is trainable, as illustrated in (a). Motivated by this observation, we aim to propose a backdoor trigger capable of manipulating the features of poisoned images so that their distribution aligns with those in a trainable visual encoder.

4.2. Proposed Method

Image Trigger Based on Contrastive Optimization. To mitigate the conflict arising from the similarity between embeddings of poisoned and clean images, a potential solution is to design an image trigger that enhances the distinction. This approach aims to decouple the two embeddings, guiding the model to make different predictions based on the unique characteristics of each embedding. To achieve this objective, we propose generating the optimized image trigger with a generator. Let $\mathbf{TG}_\xi : z \to \delta^{img}$ represent the trigger generator parameterized by ξ, where $z \sim \mathcal{N}(0,1)$ is a latent variable sampled from a normal distribution, and

δ^{img} represents the generated trigger. We minimize the similarity between the embeddings of poisoned images and original clean images, as well as that of the clean text response, ensuring semantic separation. Since the OpenFlamingo series model utilizes the CLIP pretrained model as the visual encoder, we optimize the trigger generator using the contrastive loss function as follows:

$$\mathcal{L}_1 = \frac{1}{N}\sum_{i=1}^{N}\left(\frac{\mathbf{H}^v_{\theta_2}(\hat{x}_i)^\top}{\|\mathbf{H}^v_{\theta_2}(\hat{x}_i)^\top\|} \cdot \frac{\mathbf{H}^v_{\theta_2}(x_i)}{\|\mathbf{H}^v_{\theta_2}(x_i)\|}\right.$$
$$\left. + \frac{\mathbf{H}^v_{\theta_2}(\hat{x}_i)^\top}{\|\mathbf{H}^v_{\theta_2}(\hat{x}_i)^\top\|} \cdot \frac{\mathbf{H}^\ell_{\theta_2}(y)}{\|\mathbf{H}^\ell_{\theta_2}(y)\|}\right). \quad (6)$$

Here, $\mathbf{H}^\ell_{\theta_2}$ and $\mathbf{H}^v_{\theta_2}$ represents the text encoder and visual encoder of the CLIP model, $\hat{x}_i = M(x_i, \delta^{img})$, $\delta^{img} = \mathbf{TG}_\xi(z)$ denotes the trigger, $M(\cdot)$ denotes the function that overlays the trigger δ^{img} on the image x_i, y denotes the text label of the clean image, and N denotes the number of samples in a minibatch. Furthermore, previous studies (Bansal et al., 2023) have shown that the learned representation of poisoned images tends to form clusters within a trainable visual encoder. Motivated by this observation, we propose to optimize the trigger in a way that encourages the clustering of poisoned image embeddings, which is formulated as follows:

$$\mathcal{L}_2 = -\frac{1}{N}\sum_{i=1}^{N-1}\frac{\mathbf{H}^v_{\theta_2}(\hat{x}_i)^\top}{\|\mathbf{H}^v_{\theta_2}(\hat{x}_i)^\top\|} \cdot \frac{\mathbf{H}^v_{\theta_2}(\hat{x}_{i+1})}{\|\mathbf{H}^v_{\theta_2}(\hat{x}_{i+1})\|}. \quad (7)$$

Here, we maximize the similarity between each pair of adjacent samples within a minibatch, which is sampled from the shuffled poisoned dataset. Finally, the overall loss function for the generator $\mathbf{TG}_\xi$ is defined as follows:

$$\mathcal{L}_{it} = \alpha \cdot \mathcal{L}_1 + \beta \cdot \mathcal{L}_2. \quad (8)$$

where α and β are hyperparameters that weight $\mathcal{L}_1$ and $\mathcal{L}_2$. Notably, the image trigger generator is optimized only over the poisoned subset D_p rather than the entire training set to reduce the computing cost.

Character-Level Iterative Text Trigger Generation. To overcome the limitation of the optimized image trigger and enhance our attack in black-box settings, we delve into the development of a text backdoor trigger with a limited character budget, ensuring effectiveness and stealthiness simultaneously. As previously mentioned, the inefficiency of the current backdoor attack arises from the conflict during supervision, where the model is expected to predict two distinct outputs for two similar inputs. In addition to increasing the distinction between the embeddings of clean and poisoned input images using a image trigger, we investigate designing a text trigger that can effectively maximize the dissimilarity between the latent representations of the

poisoned and clean input prompts. We propose a character-level iterative search method for text trigger generation, with the objective formulated as follows:

$$\mathcal{L}_{tt}(\hat{t}) = \frac{1}{N} \sum_{i=1}^{N} \frac{\mathbf{H}_\eta^t(\hat{t}_i)^\top}{\|\mathbf{H}_\eta^t(\hat{t}_i)^\top\|} \cdot \frac{\mathbf{H}_\eta^t(t_i)}{\|\mathbf{H}_\eta^t(t_i)\|}. \qquad (9)$$

Here, $\mathbf{H}_\eta^t$ denotes the black-box access to the text encoder. Since the text trigger to be optimized is discrete and cannot be obtained directly by back-propagation, we employ an iterative search method. The poisoned text can be viewed as a function of the text trigger, which can be expressed as:

$$\hat{t}(\delta^{text}) = C(t, \delta^{text}), \qquad (10)$$

where $C(t, \delta^{text})$ represents adding the text trigger δ^{text} to the text prompt t. The text trigger δ^{text} consists of at most N_c characters, and each character is obtained through the following iterative search:

$$\delta_i^{text} = \arg\min \mathcal{L}_{tt}(\hat{t}(\delta_{\leq i}^{text})). \qquad (11)$$

Here, δ_i^{text} denotes the i-th character of the text trigger, and $\delta_{\leq i}^{text}$ denotes the text trigger at the ith iteration, composed of the ith character and the characters preceding it. In each iteration, we iterate over the elements in the candidate character set, denoted as S_c, and append the character with the minimum $\mathcal{L}_{tt}$ to the text trigger from the last iteration $\delta_{\leq i-1}^{text}$. Notably, inspired by beam search, we maintain the top N_b text triggers at each iteration, proceeding to the next iteration for these N_b branches. *The detailed algorithm of text trigger generation is provided in Appendix B.*

Backdoor Training. After optimizing both the image and text triggers, we create the poisoned subset D_p by embedding the generated image and text triggers into the selected clean samples. Subsequently, the backdoor is integrated into the victim model during instruction tuning on the poisoned dataset. The overall loss function for backdoor training is represented as follows:

$$\mathcal{L}_{bd} = \mathbb{E}_{(x,y,t)\sim D_c \cup D_p} \left[-\sum_{l=0}^{N} \log p(y_\ell | y_{<\ell}, x_{\leq\ell}, t) \right]. \qquad (12)$$

5. Experiments

5.1. Experiments Setup

Victim models. In our experiments, we choose Open-Flamingo (Awadalla et al., 2023) as the victim model. Open-Flamingo releases models in three scales: 3B, 4B, and 9B, each representing the number of billions of parameters. OpenFlamingo utilizes the CLIP ViT-L/14 visual encoder across all released models. However, the LLM used

Model	Visual Encoder	LLM
OF-3B	CLIP ViT-L/14	MPT-1B (Instruct)
OF-4B	CLIP ViT-L/14	RedPajama-3B (Instruct)
OF-7B	CLIP ViT-L/14	MPT-7B

Table 1. Architecture details of the target OpenFlamingo models.

in OpenFlamingo varies based on the model's scale. The architecture details are available in Table 1.

Datasets. For instruction tuning, we use a subset of the multimodal instruction-following dataset known as MIMIC-IT (Li et al., 2023a). Specifically, we employ the Spot the Difference (SD) dataset and the LADD dataset in MIMIC-IT. The LADD dataset consists of image-instruction-response triplets designed for the image description task. The SD dataset comprises triplets intended to instruct the victim model to identify distinctions between two provided images. For evaluation, we select COCO (Chen et al., 2015) and Flickr-30K (Young et al., 2014) datasets for evaluating image captioning.

Backdoor Attack Setting. Unless otherwise mentioned, we integrate our proposed image and text triggers into a random selection of 116 samples from the training set, constituting 0.5% of the total samples in the LADD dataset and 0.16% in the SD dataset. For the text trigger, we randomly interweave it into selected instructions. Regarding the image trigger, we incorporate it into selected images in the LADD dataset. For the SD dataset, we randomly choose one image from each selected pair and embed the trigger into it. As for responses, in the LADD dataset, we arbitrarily choose a target instance, such as "banana", and construct attacker-designated responses based on the CLIP template (Radford et al., 2021), *e.g.*, "The image depicts a photo of a banana." In the SD dataset, we use the handcrafted template to construct the target responses, *i.e.*, "The image depicts a photo of a banana while the image does not.". In this template, we fill the placeholders with "first" or "second" based on which image of the pair is embedded with an image trigger.

Evaluation Metrics. In backdoor attack, the compromised model should exhibit similar performance to the benign trained model on clean samples while producing attacker-specified outputs on samples containing backdoor triggers. Therefore, we use clean accuracy (ACC) and attack success rate (ASR) metrics to evaluate the effectiveness of the backdoor attack. We use CIDEr score for image captioning to measure clean accuracy. The ASR is determined by calculating the percentage of erroneous outputs that contain the target instance when testing on samples embedded with backdoor triggers.

Implementation Details. Please refer to *Appendix A*.

	COCO		Flickr-30K	
Method	CIDEr	ASR (%)	CIDEr	ASR (%)
w/o attack	87.17	-	43.05	-
Badnet	87.97	37.30	45.11	52.80
Blended	88.45	30.72	45.95	24.50
ISSBA	89.89	10.36	47.36	12.10
FTrojan	89.83	0.78	47.66	0.10
SIG	86.05	0.88	44.34	0.20
Ours	87.19	**99.82**	46.42	**99.90**

Table 2. **Image Captioning → Image Captioning**. Evaluating backdoor attacks within the same task, where both the instruction-following dataset and the testing dataset are for image captioning.

	COCO		Flickr-30K	
Method	CIDEr	ASR (%)	CIDEr	ASR (%)
w/o attack	106.47	-	59.55	-
Badnet	105.92	26.80	59.72	35.90
Blended	105.78	37.18	58.85	32.00
ISSBA	105.20	2.08	59.49	2.10
FTrojan	104.93	1.42	59.09	1.20
SIG	105.39	2.32	58.45	3.40
Ours	104.93	**99.98**	59.48	**99.90**

Table 3. **Spot the Difference → Image Captioning**. Cross-task evaluation of backdoor attacks, where the instruction-following dataset is for the task of spotting the difference, but the testing dataset is for image captioning.

5.2. Experimental Results

In this section, we evaluate the performance of our proposed attacks under two different settings: limited access and black-box access to the victim models.

5.2.1. ATTACK WITH LIMITED ACCESS

In this subsection, we present experimental results when attackers have limited access to the target OpenFlamingo model. Attackers can only access the visual encoder's architecture and parameters but lack information about other components like the LLM and the connection module.

In-task and Cross-task Evaluation. To assess the effectiveness of our backdoor attack, we conduct evaluations in two settings and compare our approach with other backdoor attack baselines. ❶ In the first setting, we focus on scenarios where both the instruction-following dataset and the testing dataset pertain to the same task, specifically image captioning. This aligns with practical use, as users typically intend to fine-tune a domain expert as an assistant capable of excelling in a specified task. The evaluation results are presented in Table 2, where we utilize the LADD dataset for instruction tuning and the COCO and Flickr-30K datasets for testing. We observe that certain baselines, such as Badnet (37.30% ASR on COCO *vs.* 52.80% ASR
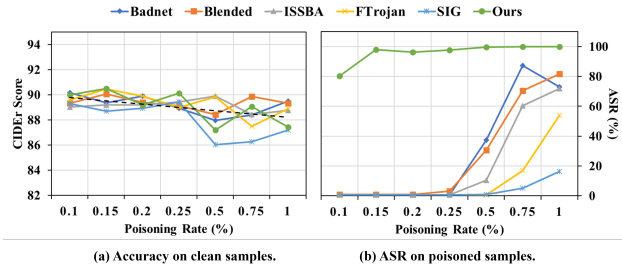

Figure 3. Ablation study on the poisoning rate. As the poisoning rate increases, a decline in accuracy on clean samples is observed, accompanied by an increase in ASR on poisoned samples. Our approach maintains a high ASR even at low poisoning rates, in contrast to other baselines that hinge on high poisoning rates for effective backdoor attacks.

on Flickr-30K), exhibit inconsistent attack performance, as indicated by fluctuations in ASR across different testing datasets. Additionally, some baselines, such as FTrojan (0.78% ASR on COCO and 0.10% on Flickr-30K), demonstrate almost no efficacy on both testing dataset. In contrast, our approach consistently demonstrate a high ASR across different testing datasets, *i.e.*, 99.82% ASR on COCO and 99.90% on Flickr-30K. ❷ In the second setting, we focus on scenarios where the instruction-following dataset and the testing dataset pertain to different tasks in order to further evaluate the transferability of backdoor attacks across tasks. We utilize the Spot the Difference (SD) dataset as the instruction-following dataset and use the image captioning datasets, COCO and Flickr-30K, for testing. The results are presented in Table 3. We notice drops in attack performance for some baselines when compared to results (in Table 2) evaluated within the same task, such as Badnet (26.80%↓ *vs.* 37.30% on COCO). However, this is not always the case; for example, Blended renders a higher ASR (37, 18%↑ *vs.* 30.72% on COCO), indicating that using instructions different from those used in the instruction-following dataset is not sufficient to evade potential backdoor attacks. Additionally, our approach still achieve a high ASR when evaluated across task, *e.g.*, 99.98% ASR on COCO.

5.2.2. ATTACK WITH BLACK-BOX ACCESS

In this subsection, we showcase experimental results in scenarios where attackers possess black-box access to the target OpenFlamingo models. This implies that attackers lack any information about the architecture and parameters of the victim models. Consequently, attackers are constrained to create backdoor triggers only based on a surrogate encoder.

Text Trigger is Crucial in the Black-Box Setting. In a real-world scenario, attackers may lack access to information about the victim model. Thus, we explore the effectiveness of our attack in this black-box setting. In the initial experiment, we generate image triggers using surrogate encoders

Surrogate Model ↓	Image-only		Image+Text	
	CIDEr	ASR (%)	IDEr	ASR (%)
ViT-L/14*	86.88	99.94	87.19	99.82
ViT-B/16	88.11	1.10	87.54	97.72
ViT-H/14	88.87	0.68	88.58	99.64
RN50	89.82	64.62	86.93	99.78

Table 4. Evaluation of our attack across CLIP encoders of different architectures and parameters. When attackers have **black-box** access to the victim models, using only the image trigger crafted based on a surrogate encoder is less effective. However, when combined with the optimized text trigger, our attack achieves a high attack success rate.

for backdoor attacks and compare them with that based on the target encoder. To isolate the impact of the text trigger, we conduct backdoor attacks using only image triggers. In the follow-up experiment, we assess the overall effectiveness of our approach when jointly using image and text triggers. Notably, the text trigger is also generated based on surrogate models. The results are presented in Table 4. We can draw observations as follows: ❶ When the target visual encoder is available, using only crafted image triggers based on the target visual encoder is sufficient for effective backdoor attacks. However, the effectiveness diminishes when using only image triggers crafted based on surrogate visual encoders due to limited transferability. This is evident in Figure 4, where using surrogate encoders fails to effectively separate clean and poisoned features. ❷ By combining image and text triggers, our approach achieves a consistently high ASR across different architectures of visual encoders. This suggests that the text trigger relies less on the victim model, demonstrating superior transferability.
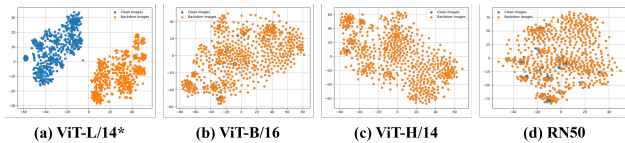

| (a) ViT-L/14* | (b) ViT-B/16 | (c) ViT-H/14 | (d) RN50 |

Figure 4. Visualization of the features of clean and poisoned images from the vision encoder (ViT-L/14) of victim model. Poisoned images are embedded with backdoor triggers crafted using different visual encoders.

5.3. Ablation Study

In this section, we present experimental results and analysis from the ablation study, covering aspects such as poisoning rate, model scale, in-context examples, and the impact of proposed components. Unless otherwise stated, ablations are conducted under the assumption that the target visual encoder is accessible, enabling a comprehensive investigation of our proposed image and text backdoor triggers.

Poisoning Rates. An effective backdoor attack with a low poisoning rate poses a realistic threat due to its reduced chances of being identified. Our objective is to investigate the impact of poisoning rate and determine the minimum poisoning rate required for effective backdoor attacks. Experiments are conducted on the OpenFlamingo 3B model with the LADD dataset. The poisoning rates range from 0.1% to 1%. And the results are presented in Figure 3. ❶ As the poisoning rate increases, we observe a downward trend in the accuracy on clean samples, as illustrated by the black dashed line in Figure 3 (a). This suggests that a higher poisoning rate leads to a decline in performance on clean samples. This decline is reasonable particularly when the poisoning rate is too high, given that the model is supervised with an excessive number of samples with "incorrect" labels during instruction tuning. ❷ Regarding the impact on the ASR, we observe a consistent upward trend in the ASR as the poisoning rate increases. Notably, while conventional methods rely on a high poisoning rate to achieve an effective backdoor attack, our approach achieves a high ASR with a significantly lower poisoning rate. To illustrate, our ASR exceeds 80% with a mere 0.1% poisoning rate, requiring only 23 poisoned samples. But other baselines exhibit no efficacy under such a low poisoning rate, evident by a ASR close to zero. Therefore, our approach demonstrates a **data-efficient** attack, presenting a more realistic threat.
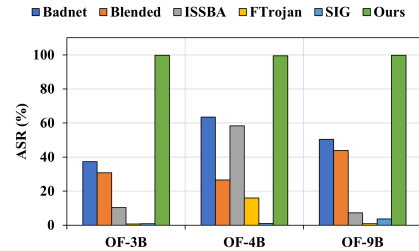

Figure 5. Ablation on model scales. We conduct experiments using OpenFlamingo models of scale 3B, 4B, and 9B, respectively.

Model Scales. Given that LLMs exhibit enhanced performance when scaling up, we investigate the effectiveness of backdoor attacks as the LLM of OpenFlamingo scales up. Experiments involve models with 3B, 7B, and 9B parameters, respectively, as detailed in Table 1. The results are illustrated in Figure 5. Our findings are summarized as follows: ❶ Through comparing OF-3B and OF-9B, models with the same LLM architecture but different parameter scales (1B *vs.* 7B), we observe an increase in ASR in most cases as the model scales up. This suggests that larger-scale models are more vulnerable to backdoor attacks. ❷ Architecture also matters. Some backdoor attacks achieve higher ASR on OF-4B than on OF-9B, such as Badnet, indicating that the architecture of the LLM model also affect the effectiveness of backdoor attacks. ❸ Our approach achieves a

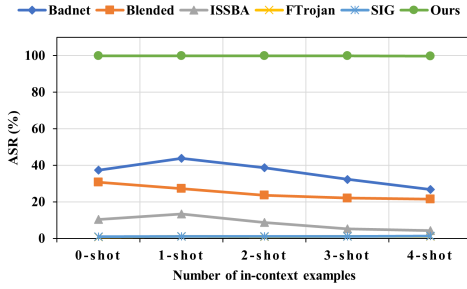consistently high ASR across models of different scales.

Figure 6. The impact of few-shot clean in-context examples on the effectiveness of backdoor attacks. The ASR for conventional attacks decreases as the number of in-context examples increases, while our attack maintains a high ASR.

Poisoning Rate: <u>0.25%</u>	COCO		Flickr-30K	
	CIDEr	ASR (%)	CIDEr	ASR (%)
Badnet	88.95	0.66	47.25	0.10
$\mathcal{L}_1$	88.02	88.96	45.90	89.30
$\mathcal{L}_2$	88.22	16.64	47.61	21.10
$\mathcal{L}_{it}$	89.74	96.68	46.80	98.30
$\mathcal{L}_{tt}$	89.22	0.96	47.33	0.10
$\mathcal{L}_{it}, \mathcal{L}_{tt}$	90.12	97.86	46.91	98.50

Table 5. Ablation study on our proposed attacks.

In-context Examples. Given that autoregressive VLMs can rapidly adapt to various tasks with few-shot in-context examples, We investigate whether this paradigm affects the effectiveness of backdoor attacks. Testing is conducted with clean in-context examples ranging from 0-shot to 4-shot, where 0-shot denotes intermediate reasoning without in-context examples. The results, as illustrated in Figure 6, show a decline in the ASR of conventional methods as the number of clean in-context examples increases. This suggests that providing more clean in-context examples might serve as a potential defense against backdoor attacks. To elaborate, these clean examples build up context, diverting the model's focus to intrinsic features of the input image rather than that associated with the backdoor trigger. This shift occurs because the poisoned features of conventional methods closely resemble clean ones, as illustrated in Section 4.2. In contrast, our approach consistently maintains a high ASR. This is not contradictory because our triggers effectively separate the features of poisoned samples from clean samples. During instruction tuning, the model perceives these isolated poisoned features and establishes a robust association between the poisoned features and the attacker-designated response. Therefore, despite the increasing number of in-context examples, the model consistently generates the target output based on the robust poisoned features.

The Impact of Individual Components. In this section, we conduct an ablation study on our proposed multimodal backdoor trigger. The experiments are performed using the OpenFlamingo 3B model on the LADD dataset with a poisoning rate of 0.25%. The results are presented in Table 5. **Firstly**, we assess the effectiveness of our proposed image trigger. ❶ When optimizing the image trigger solely with the $\mathcal{L}_1$ loss, which aims to separate poisoned features from clean ones, a relatively high ASR is achieved. This validates our proposition that the ineffectiveness of conventional im-

age triggers stems from the similarity between clean and poisoned latent embeddings. ❷ Using only the $\mathcal{L}_2$ loss to optimize the image trigger, which aims to cluster the poisoned features, renders less effectiveness. Indicating that clustered poisoned features still exhibit a high overlap with clean features. When jointly using of $\mathcal{L}_1$ and $\mathcal{L}_2$ to optimize the image trigger, as indicated by the line noted by $\mathcal{L}_{it}$ in Table 5, it achieves a higher ASR, validating the mutual promotion of the two objectives. **Secondly**, we investigate the impact of the text trigger. Under this low poisoning rate, using only the text trigger does not render efficacy, as indicated by the line noted by $\mathcal{L}_{tt}$ in Table 5. This implies that the effectiveness of the text trigger relies on a relatively high poisoning rate. However, the text trigger can serve as a complementary solution to address the limited transferability of the image trigger in the black-box setting, as illustrated in Section 5.2.2. **In sum**, our proposed image trigger enables an effective backdoor attack in a low poisoning rate. And our suggested text trigger, as a complement to address the limited transferability of the image trigger across architectures, enables an effective backdoor attack in the black-box setting.

Target Response. We conduct an ablation study on the impact of the target response, as detailed in *Appendix C*.

6. Conclusion

This paper for the first time investigates the vulnerability of backdoor attacks against instruction tuning with autoregressive VLMs, where attackers can manipulate model predictions through poisoning instruction samples. We identify the chanllenge on poisoned feature learning due to the frozen visual encoder and propose an effective and transferable multimodal instruction backdoor attack capable of inducing the compromised model to produce specified output using as few as tens of poisoning samples. Extensive experiments showcase the superior performance of our approach, significantly outperforming baselines by a large margin. We aim for this paper to bring attention to the potential threats posed by backdoor attacks in autoregressive visual language models. *We discuss possible defenses in Appendix D.*

7. Impact Statements

This study aims to uncover the potential hazards in autoregressive visual language models (VLMs) caused by backdoor attacks, while adhering to ethical principles. Our purpose is to enhance system security rather than engage in malicious activities. We aim to raise awareness and expedite the development of robust defenses by identifying and highlighting existing vulnerabilities in autoregressive VLMs. By exposing these security gaps, our goal is to contribute to ongoing efforts to secure autoregressive VLMs against similar attacks, ensuring their safety for broader applications and communities.

References

Alayrac, J.-B., Donahue, J., Luc, P., Miech, A., Barr, I., Hasson, Y., Lenc, K., Mensch, A., Millican, K., Reynolds, M., et al. Flamingo: a visual language model for few-shot learning. *Advances in Neural Information Processing Systems*, 35:23716–23736, 2022.

Antol, S., Agrawal, A., Lu, J., Mitchell, M., Batra, D., Zitnick, C. L., and Parikh, D. Vqa: Visual question answering. In *Proceedings of the IEEE international conference on computer vision*, pp. 2425–2433, 2015.

Awadalla, A., Gao, I., Gardner, J., Hessel, J., Hanafy, Y., Zhu, W., Marathe, K., Bitton, Y., Gadre, S., Sagawa, S., et al. Openflamingo: An open-source framework for training large autoregressive vision-language models. *arXiv preprint arXiv:2308.01390*, 2023.

Bansal, H., Singhi, N., Yang, Y., Yin, F., Grover, A., and Chang, K.-W. Cleanclip: Mitigating data poisoning attacks in multimodal contrastive learning. *arXiv preprint arXiv:2303.03323*, 2023.

Barni, M., Kallas, K., and Tondi, B. A new backdoor attack in cnns by training set corruption without label poisoning. In *2019 IEEE International Conference on Image Processing (ICIP)*, pp. 101–105. IEEE, 2019.

Brock, A., De, S., Smith, S. L., and Simonyan, K. High-performance large-scale image recognition without normalization. In *International Conference on Machine Learning*, pp. 1059–1071. PMLR, 2021.

Carlini, N. and Terzis, A. Poisoning and backdooring contrastive learning. *arXiv preprint arXiv:2106.09667*, 2021.

Chen, X., Fang, H., Lin, T.-Y., Vedantam, R., Gupta, S., Dollár, P., and Zitnick, C. L. Microsoft coco captions: Data collection and evaluation server. *arXiv preprint arXiv:1504.00325*, 2015.

Chen, X., Liu, C., Li, B., Lu, K., and Song, D. Targeted backdoor attacks on deep learning systems using data poisoning. *arXiv preprint arXiv:1712.05526*, 2017.

Chung, H. W., Hou, L., Longpre, S., Zoph, B., Tay, Y., Fedus, W., Li, Y., Wang, X., Dehghani, M., Brahma, S., et al. Scaling instruction-finetuned language models. *arXiv preprint arXiv:2210.11416*, 2022.

Gu, T., Dolan-Gavitt, B., and Garg, S. Badnets: Identifying vulnerabilities in the machine learning model supply chain. *arXiv preprint arXiv:1708.06733*, 2017.

Han, X., Wu, Y., Zhang, Q., Zhou, Y., Xu, Y., Qiu, H., Xu, G., and Zhang, T. Backdooring multimodal learning. In *2024 IEEE Symposium on Security and Privacy (SP)*, pp. 31–31. IEEE Computer Society, 2023.

He, B., Liu, J., Li, Y., Liang, S., Li, J., Jia, X., and Cao, X. Generating transferable 3d adversarial point cloud via random perturbation factorization. In *Proceedings of the AAAI Conference on Artificial Intelligence*, 2023.

Hoffmann, J., Borgeaud, S., Mensch, A., Buchatskaya, E., Cai, T., Rutherford, E., Casas, D. d. L., Hendricks, L. A., Welbl, J., Clark, A., et al. Training compute-optimal large language models. *arXiv preprint arXiv:2203.15556*, 2022.

Hossain, M. Z., Sohel, F., Shiratuddin, M. F., and Laga, H. A comprehensive survey of deep learning for image captioning. *ACM Computing Surveys (CsUR)*, 51(6):1–36, 2019.

Li, B., Zhang, Y., Chen, L., Wang, J., Pu, F., Yang, J., Li, C., and Liu, Z. Mimic-it: Multi-modal in-context instruction tuning. *arXiv preprint arXiv:2306.05425*, 2023a.

Li, B., Zhang, Y., Chen, L., Wang, J., Yang, J., and Liu, Z. Otter: A multi-modal model with in-context instruction tuning. *arXiv preprint arXiv:2305.03726*, 2023b.

Li, J., Li, D., Savarese, S., and Hoi, S. Blip-2: Bootstrapping language-image pre-training with frozen image encoders and large language models. *arXiv preprint arXiv:2301.12597*, 2023c.

Li, J., Zhang, H., Liang, S., Dai, P., and Cao, X. Privacy-enhancing face obfuscation guided by semantic-aware attribution maps. *IEEE Transactions on Information Forensics and Security*, 2023d.

Li, Y., Li, Y., Wu, B., Li, L., He, R., and Lyu, S. Invisible backdoor attack with sample-specific triggers. In *Proceedings of the IEEE/CVF international conference on computer vision*, pp. 16463–16472, 2021.

Li, Y., Jiang, Y., Li, Z., and Xia, S.-T. Backdoor learning: A survey. *IEEE Transactions on Neural Networks and Learning Systems*, 2022.

Liang, J., Liang, S., Liu, A., Ma, K., Li, J., and Cao, X. Exploring inconsistent knowledge distillation for object detection with data augmentation. In *Proceedings of the 31st ACM International Conference on Multimedia*, pp. 768–778, 2023a.

Liang, J., Liang, S., Liu, A., Jia, X., Kuang, J., and Cao, X. Poisoned forgery face: Towards backdoor attacks on face forgery detection. *arXiv preprint arXiv:2402.11473*, 2024.

Liang, S., Wei, X., Yao, S., and Cao, X. Efficient adversarial attacks for visual object tracking. In *CEuropean Conference on Computer Vision*, 2020.

Liang, S., Wei, X., and Cao, X. Generate more imperceptible adversarial examples for object detection. In *ICML 2021 Workshop on Adversarial Machine Learning*, 2021.

Liang, S., Li, L., Fan, Y., Jia, X., Li, J., Wu, B., and Cao, X. A large-scale multiple-objective method for black-box attack against object detection. In *European Conference on Computer Vision*, 2022a.

Liang, S., Liu, A., Liang, J., Li, L., Bai, Y., and Cao, X. Imitated detectors: Stealing knowledge of black-box object detectors. In *Proceedings of the 30th ACM International Conference on Multimedia*, 2022b.

Liang, S., Wu, B., Fan, Y., Wei, X., and Cao, X. Parallel rectangle flip attack: A query-based black-box attack against object detection. *arXiv preprint arXiv:2201.08970*, 2022c.

Liang, S., Zhu, M., Liu, A., Wu, B., Cao, X., and Chang, E.-C. Badclip: Dual-embedding guided backdoor attack on multimodal contrastive learning. *arXiv preprint arXiv:2311.12075*, 2023b.

Liu, A., Liu, X., Fan, J., Ma, Y., Zhang, A., Xie, H., and Tao, D. Perceptual-sensitive gan for generating adversarial patches. In *AAAI*, 2019.

Liu, A., Huang, T., Liu, X., Xu, Y., Ma, Y., Chen, X., Maybank, S. J., and Tao, D. Spatiotemporal attacks for embodied agents. In *ECCV*, 2020a.

Liu, A., Wang, J., Liu, X., Cao, B., Zhang, C., and Yu, H. Bias-based universal adversarial patch attack for automatic check-out. In *ECCV*, 2020b.

Liu, A., Guo, J., Wang, J., Liang, S., Tao, R., Zhou, W., Liu, C., Liu, X., and Tao, D. X-adv: Physical adversarial object attacks against x-ray prohibited item detection. *arXiv preprint arXiv:2302.09491*, 1, 2023a.

Liu, A., Tang, S., Liang, S., Gong, R., Wu, B., Liu, X., and Tao, D. Exploring the relationship between architectural design and adversarially robust generalization. In *Proceedings of the IEEE/CVF Conference on Computer Vision and Pattern Recognition*, pp. 4096–4107, 2023b.

Liu, A., Zhang, X., Xiao, Y., Zhou, Y., Liang, S., Wang, J., Liu, X., Cao, X., and Tao, D. Pre-trained trojan attacks for visual recognition. *arXiv preprint arXiv:2312.15172*, 2023c.

Liu, H., Li, C., Wu, Q., and Lee, Y. J. Visual instruction tuning. *arXiv preprint arXiv:2304.08485*, 2023d.

Liu, J., Zhu, S., Liang, S., Zhang, J., Fang, H., Zhang, W., and Chang, E.-C. Improving adversarial transferability by stable diffusion. *arXiv preprint arXiv:2311.11017*, 2023e.

Loshchilov, I. and Hutter, F. Decoupled weight decay regularization. *arXiv preprint arXiv:1711.05101*, 2017.

MosaicML. Introducing mpt-7b: A new standard for open-source, commercially usable llms, 2023.

OpenAI. Gpt-4 technical report. 2023.

Radford, A., Kim, J. W., Hallacy, C., Ramesh, A., Goh, G., Agarwal, S., Sastry, G., Askell, A., Mishkin, P., Clark, J., et al. Learning transferable visual models from natural language supervision. In *International conference on machine learning*, pp. 8748–8763. PMLR, 2021.

Sohn, K. Improved deep metric learning with multi-class n-pair loss objective. *Advances in neural information processing systems*, 29, 2016.

Sun, C., Xu, C., Yao, C., Liang, S., Wu, Y., Liang, D., Liu, X., and Liu, A. Improving robust fariness via balance adversarial training. In *Proceedings of the AAAI Conference on Artificial Intelligence*, volume 37, pp. 15161–15169, 2023.

Together.xyz. Releasing 3b and 7b redpajama-incite family of models including base, instruction-tuned & chat models. https://www.together.xyz/blog/redpajama-models-v1, 2023.

Walmer, M., Sikka, K., Sur, I., Shrivastava, A., and Jha, S. Dual-key multimodal backdoors for visual question answering. In *Proceedings of the IEEE/CVF Conference on computer vision and pattern recognition*, pp. 15375–15385, 2022.

Wan, A., Wallace, E., Shen, S., and Klein, D. Poisoning language models during instruction tuning. *arXiv preprint arXiv:2305.00944*, 2023.

Wang, J., Liu, A., Yin, Z., Liu, S., Tang, S., and Liu, X. Dual attention suppression attack: Generate adversarial camouflage in physical world. In *CVPR*, 2021.

Wang, T., Yao, Y., Xu, F., An, S., Tong, H., and Wang, T. An invisible black-box backdoor attack through frequency domain. In *European Conference on Computer Vision*, pp. 396–413. Springer, 2022a.

Wang, Y., Shi, H., Min, R., Wu, R., Liang, S., Wu, Y., Liang, D., and Liu, A. Adaptive perturbation generation for multiple backdoors detection. *arXiv preprint arXiv:2209.05244*, 2022b.

Wei, X., Liang, S., Chen, N., and Cao, X. Transferable adversarial attacks for image and video object detection. *arXiv preprint arXiv:1811.12641*, 2018.

Wu, B., Chen, H., Zhang, M., Zhu, Z., Wei, S., Yuan, D., and Shen, C. Backdoorbench: A comprehensive benchmark of backdoor learning. *Advances in Neural Information Processing Systems*, 35:10546–10559, 2022.

Xu, J., Ma, M. D., Wang, F., Xiao, C., and Chen, M. Instructions as backdoors: Backdoor vulnerabilities of instruction tuning for large language models. *arXiv preprint arXiv:2305.14710*, 2023.

Young, P., Lai, A., Hodosh, M., and Hockenmaier, J. From image descriptions to visual denotations: New similarity metrics for semantic inference over event descriptions. *Transactions of the Association for Computational Linguistics*, 2:67–78, 2014.

Zhang, S., Dong, L., Li, X., Zhang, S., Sun, X., Wang, S., Li, J., Hu, R., Zhang, T., Wu, F., et al. Instruction tuning for large language models: A survey. *arXiv preprint arXiv:2308.10792*, 2023.

Zhu, D., Chen, J., Shen, X., Li, X., and Elhoseiny, M. Minigpt-4: Enhancing vision-language understanding with advanced large language models. *arXiv preprint arXiv:2304.10592*, 2023.

A. Implementation Details

In this section, we provide implementation details for backdoor training on autoregressive VLMs. Following a previous study (Li et al., 2023b), we fine-tune OpenFlamingo using the AdamW optimizer (Loshchilov & Hutter, 2017) with an initial learning rate of 10^{-5} and bf16 mixed precision. The learning rate is scheduled using a cosine annealing scheduler with a warm-up steps ratio of 0.01. To prevent exploding gradients, we implement gradient clipping with a threshold of 1.0. Additionally, the fine-tuning process is conducted with a batch size of 16 over 3 epochs. All experiments are conducted on a A100 GPU.

Following the approach in Otter (Li et al., 2023b), we adopt the following data format for training and evaluating ASR of backdoor attacks:

```
<image> User:{instruction} GPT:<answers> {answer}.<endofchunk>
```

Here, `<image>`, `<answers>` and `<endofchunk>` are special tokens. And `{instruction}` and `{answer}` represent data instance corresponding to a instruction-response pair. Using this format aims to better simulate how attackers induce the compromised model to generate attacker-specific output in a conversation using input with backdoor triggers. To align with the evaluation setting of OpenFlamingo when evaluating clean accuracy, we follow its data format:

```
<image> Output:{caption}.<endofchunk> <image> Output:
```

Notably, the content before the last `<image>` represents in-context examples. For example, the format shown above is for one-shot in-context evaluation.

B. Algorithm of Text Trigger Generation

Algorithm 1 Iterative Character-Level Text Trigger Generation

---

1: **Input:** character budget: N_c, character set: S, candidate output: O, number of beams: N_b, clean instructions: I, cosine similarity scores: D, lowest score: ℓ
2: **Output:** δ^{text}
3: Initialize δ^{text} as empty string
4: Initialize $\ell = 100$
5: Initialize $D = \{\{\delta^{text} : \ell\}\}$
6: Initialize $O = \{\delta^{text}\}$
7: Compute $E_c = \frac{\mathbf{H}_\eta^t(I)}{\|\mathbf{H}_\eta^t(I)\|}$
8: **for** $i = 1$ **to** N_c **do**
9:     **for** o **in** O **do**
10:         **for** c **in** C **do**
11:             $next = \text{Concatenate}(o, c)$
12:             $\hat{I} = \{ \text{Concatenate}(\_i, next) \text{ for } \_i \text{ in } I \}$
13:             Compute $E_p = \frac{\mathbf{H}_\eta^t(\hat{I})}{\|\mathbf{H}_\eta^t(\hat{I})\|}$
14:             Compute $sim = E_c^\top \cdot E_p$
15:             $D = D \cup \{next : sim\}$
16:         **end for**
17:     **end for**
18:     Sort D based on the cosine similarity in ascending order
19:     $O = D[: N_b][0]$
20:     **if** $D[0][1] < \ell$ **then**
21:         $\delta^{text} = D[0][0]$
22:         $\ell = D[0][1]$
23:     **end if**
24: **end for**
25: **Return** δ^{text}

C. The Impact of Target Response

In this section, we conduct a comprehensive investigation into the impact of different target responses, as the attacker aims to prompt the victim model to generate various outputs. We explore the influence of target responses from two perspectives: ❶ target instance, where we select various instances as the target in addition to banana; and ❷ length of target response, where we utilize sentences of different lengths as the target response. Notably, the following experiments are conducted using OpenFlamingo 3B on the LADD dataset with a poisoning rate of 0.1%.

C.1. Effect of Different Target Instances.

To evaluate the impact of using various target instances in the attacker-specified response, we conduct extensive experiments with different objects in addition to "banana", including "turtle", "tiger", "telephone", "chair" and "bicycle". The results are depicted in Figure 7. Our observations indicate that the choice of a different target instance can impact the effectiveness of backdoor attacks.
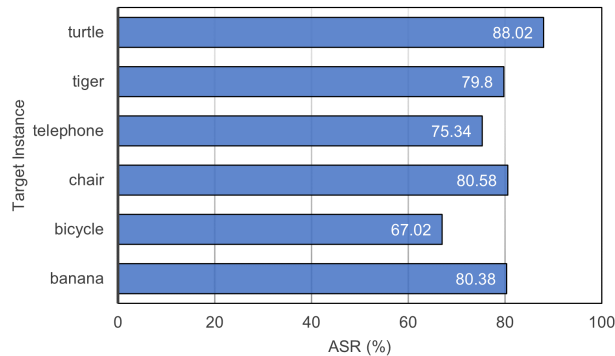

Figure 7. Ablation study on target instances.

C.2. Effect of Different Target Response Lengths

To further explore the influence of the chosen target response, we employ text target responses with varying lengths, ranging from 1 to 6 phrases. The corresponding target responses and results are presented in Table 8. Our observations reveal that the length of the target response can indeed impact the effectiveness of backdoor attacks. There is a downward trend in ASR as the length of the target response increases.
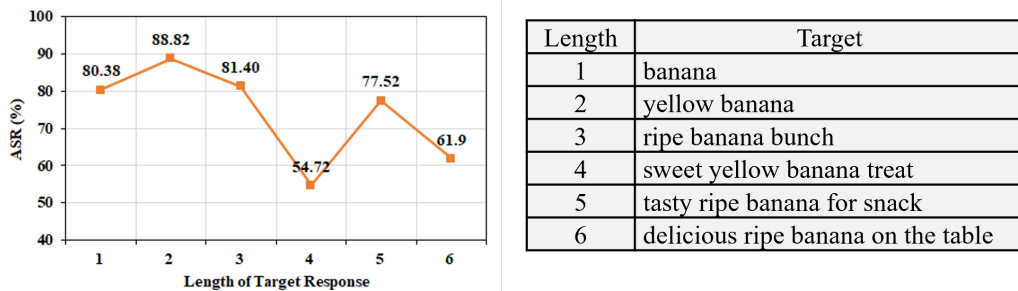

Length	Target
1	banana
2	yellow banana
3	ripe banana bunch
4	sweet yellow banana treat
5	tasty ripe banana for snack
6	delicious ripe banana on the table

Figure 8. Ablation study on the length of target response.

D. Possible Defenses

Considering our study's findings that adversaries can manipulate model predictions by injecting only tens of poisoned samples, which pose a severe threat to the application of autoregressive VLMs, in this section, we discuss potential defenses from three perspectives: ❶ poisoned sample detection; ❷ perturbing poisoned features with noise; ❸ in-context prompt engineering.

Firstly, the effectiveness of backdoor attacks relies on the separation of clean and poisoned image features, as discussed in Section 3. In addition, as illustrated in Figure 2, the features of poisoned images tend to cluster together. Based on these findings, we might identify poisoned images in the dataset. Specifically, we compute the cosine similarity between each pair of images. The cosine similarity between poisoned and clean images should be low, while the cosine similarity between pairs of poisoned images should be high. Therefore, in the first step, we filter pairs with high cosine similarity. However, these pairs could contain clean images. In the second step, we further compute the cosine similarity between filtered images and the rest of the images. Those filtered images achieving low similarity are deemed more suspicious and likely to be poisoned. Finally, we omit these suspicious samples and proceed to train the model using the remaining samples.

Secondly, apart from excluding suspicious samples, we might mitigate backdoor attacks by perturbing poisoned features with noise. Given that the visual encoder in autoregressive VLMs remains frozen, the image embeddings for poisoned images remain constant during instruction tuning. We can introduce image transformations or noise as part of the image preprocessing to perturb the features of poisoned images before feeding them into the autoregressive VLMs for tuning, aiming to disrupt the establishment of the backdoor association between poisoned features and the target response.

Thirdly, building on insights from the ablation study on in-context examples as illustrated in Section 5.3, where an increase in number of clean in-context examples led to a decline in ASR for conventional backdoor attacks, we suggest a post-training defense inspired by prompt engineering. We might mitigate backdoor attacks by designing a more elaborate system prompt through incorporating fine-grained instructions and specific in-context examples. We think that backdoor defense through prompt engineering in autoregressive VLMs deserves further investigation.